Understanding the Vortex-Ring State for VTOL Aircraft in Vertical and Steep Descending Flight

Palma Caputo[1], Hasse N. J. Dekker[2,3], Marilena D. Pavel[2], Fulvio Scarano[2]

[1]University of Naples Federico II
[2]Faculty of Aerospace Engineering, Delft University of Technology
[3]Royal Netherlands Aerospace Centre
p.caputo@tudelft.nl, h.n.j.dekker-1@tudelft.nl, m.d.pavel@tudelft.nl, f.scarano@tudelft.nl

Abstract

An experimental investigation was conducted to study the Vortex Ring State (VRS) phenomenon, a hazardous flight condition for a Vertical Take-Off and Landing aircraft (VTO) which could arise when the vehicle descent speed causes the rotor to ingest its own wake. For this, a propeller is installed in a low speed wind tunnel at Delft University of Technology in such a way to simulate a descending flight phase. Thrust measurements were performed to evaluate the effect of entering VRS on the rotor while the time averaged flow field was studied through Particle Image Velocimetry (PIV). The effect on flow pattern of having an oblique descent was also investigated. The thrust measurements showed that at certain descending speed values the propeller experiences loss of thrust. Through the mean velocity field, it was possible to observe that in pure vertical descent at moderate speed recirculating patterns installed around the disc and a "bubble" of air forms around the rotor, which then bursted. The results from flow measurements were then exploited to study the flight mechanics characteristics of a VTOL configuration resembling a helicopter in vertical descent. It was demonstrated that an increase in rotor blade collective pitch was required to arrest the vehicle descent rate.

1 Introduction

With the emerging market of Urban Air Mobility (UAM), more and more aircraft designs encompass multiple rotors as the VTOL (Vertical Take-Off and Landing) capabilities are essential. All these vehicles are prone to the Vortex Ring State (VRS) in flight descending phases. VRS is a hazardous flight condition which may arise when a helicopter (or a rotor-driven vehicle) descends vertically (or at low forward speed) into its own wake (Meijer Drees & Hendal, 1951). Entering VRS in landing when already close to the ground, for example, could translate into catastrophic crash.

Seminal literature tackling VRS problem has been published throughout the years demonstrating the dangerousness of this state for different aircraft. Amongst them, a number of publications included flight tests proving the VRS occurrence. For example, (Reeder & Gustafson, 1949) study a Sikorsky R4 helicopter which experienced pronounced vibration, violent yawing motion with roll and increased descent rate. In (Stewart, 1959) a description of VRS effects for various helicopters was provided. Usual effects that were noticed relate to an increase of vibrations and pitch-down motion. In Stewart's study some helicopters exhibited more severe degradations of performance with complete loss of control, while others experienced just mild wallowing. Stewart concluded that the increase in pitching moment during VRS was most likely due to the interaction between the fuselage and the flow. In (Jimenez, et al., 2001) it was found that the main effect of entering VRS was the sudden increase of descent rate. Despite the first instinct to increase the collective, the vehicle was insensitive to it. Nevertheless, VRS effects seemed to disappear at sufficiently high forward speed.

Wind tunnel experimental studies of the rotor aerodynamics in VRS can be found in (Azuma & Obata, 1968), (Yaggy & Mort, 1963), (Meijer Drees & Hendal, 1950), (Glauert, 1926), showing results in line with the behaviour of helicopters in free flight (general loss of thrust, increase of vibration and thrust fluctuations). Oblique descent was also studied in (Yaggy & Mort, 1963), showing that the mean loss of thrust could be lower in oblique descent for certain angles, but thrust fluctuations increased.

Another approach to study the helicopter response to VRS is by building an inflow model predicting the VRS effects, of which examples could be found on the ONERA inflow model in (Jimenez, 2002) or the Georgia Tech ring vortex model (Prasad & Chen, 2005). An explanation of the dynamics of VRS was provided in (Brand, et al., 2011), in which

the organized accumulation of the wake (in a low forward air speed descent) was the characterizing feature of VRS. Several criteria have been proposed over the years to define the VRS boundaries, i.e. the flight envelope of all possible combinations of forward and descent speed at which VRS could occur. Examples of criteria for VRS were provided in (Wolkovitch, 1971), (Peters & Chen, 1982), (Basset & Prasad, 2002), (Newman, et al., 2003).

For tiltrotors, the VRS problem showed that this unique configuration of two side-by-side rotors could cause additional flight mechanics problems: any fluctuating thrust between the left and right rotor would cause an extra roll moment. The roll-off is thus typical of tiltrotors in VRS (Jimenez, et al., 2002). The V-22 Osprey accident (Arizona, 2000) suggested that the most critical descent condition for a tilt-rotor might not be axial descent, but at a shallower angle. It was also studied the oblique descent for a tandem rotor in (Washizu, et al., 1966), where the periodicity of thrust fluctuations exhibited by the helicopter was not observable for the tandem rotor.

For quadcopter drones, more recently the VRS problem showed that, contrarily to helicopters, the quadcopters should avoid not only the VRS but also the windmill brake state (WBS) region (Talaeizadeh, et al., 2020). While in this state a helicopter would have enough lift to be controlled by switching off the motors and varying the angle of attack of the blades through the collective pitch control, turning off the motors for a quadcopter means losing controllability of it when the blade pitch cannot be changed.

From the above discussion it follows that the VRS is a dangerous condition for a VTOL as it may result in vehicle loss of altitude, high level of rotor vibrations, irregular movement of the blades and temporary vehicle loss of control effectiveness and instability. The objective of this paper is to increase the understanding of the relation between the flow topology and the flight mechanics of a small-scaled propeller in VRS conditions. To this purpose, a number of wind tunnel experiments are conducted in the low speed wind tunnel at Delft University of Technology, in which the flow is analysed using quantitative and qualitative flow visualization techniques. Subsequently, flow measurements are used to obtain the induced velocity in the disc proximity. This information is implemented into a model which simulates the 3DOF longitudinal motion of a helicopter by solving the 3DOF equations of motion.

The outline of the paper is as follows. In section 2 the experimental setup together with the measurements system and data processing is described. The thrust and flow measurements results are discussed in section 3. In section 4 the experimental wind tunnel data is used to solve the 3DOF equations of motion of a helicopter, simulating a descent.

2 Experimental setup and procedure

2.1 Propeller and wind tunnel

The experimental apparatus consists of a two-bladed propeller installed with its axis perpendicular and centred to the cross section of the low speed wind tunnel, which dimension is 60×60 cm^2. The off-the-shelf propeller has a radius $R = 76.2$ mm and a $4''$ pitch, and its model number is APC 6X4E. The thrust is in the same direction as the free-stream velocity to simulate a descent condition. In order to simulate oblique descent, the propeller is mounted on a hinge. A schematic which includes the relevant parameters is provided in Figure 1.

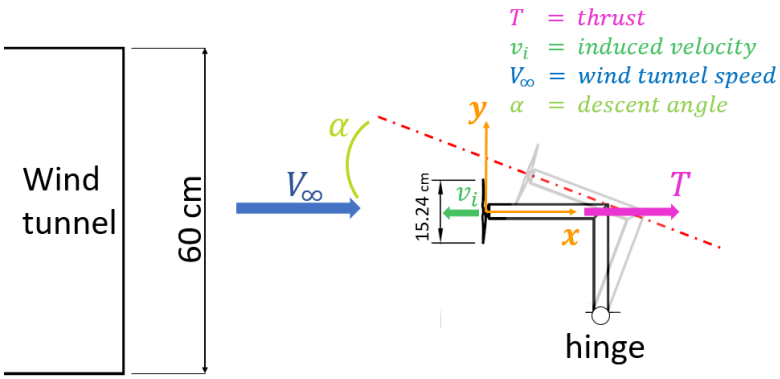

Figure 1 Schematic representation of the propeller installed in the wind tunnel with relevant parameters

2.2 Thrust measurements

The rotor is driven by a Hacker motor, type B20 26 L kv2020 + 4:1, mounted on a Futek LSB205 load cell. The rotational speed Ω is set through a JETI Box programmer, which was used to fix the maximum Ω and providing enough voltage to reach it. Both the load cell and the motor can be seen in Figure 2.

Thrust measurements were performed for different rotational speeds Ω and free stream velocity V_∞,to build thrust curves which can be used to identify trends and critical points. After having obtained the thrust curves for different Ω, it was then set to Ω=8000 RPM for the remaining experiments. The thrust data were acquired with a frequency of 2 kHz for 5 seconds, after which the time-averaged values are calculated. The thrust sensor turned out to be very sensitive to external perturbations in some configurations (oblique descent) more than others (axial descent). To evaluate the bias error, the thrust is measured before any new test and the value is then subtracted. A summary of the test conditions for the thrust measurements is provided in Table 1.

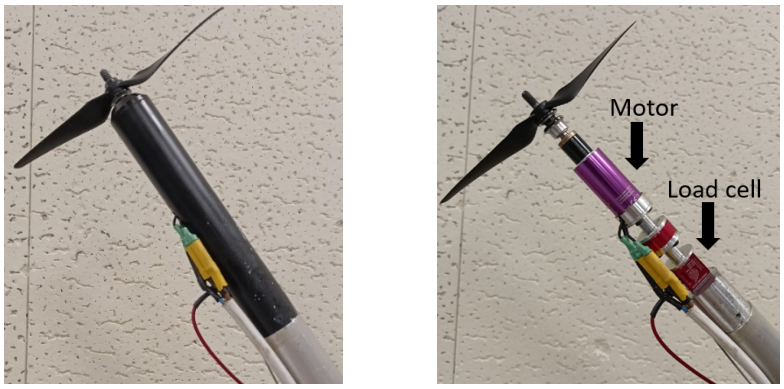

Figure 2 Propeller system. On the left: propeller with fairings; on the right: no fairings, with motor and thrust sensor (load cell)

Parameter	Value(s)
Wind tunnel speed V_∞ (m/s)	0, 0.7, 1.8, 2.9, 4, 5.1, 6.3, 7.4, 8.6, 9.8, 11, 12, 13.3
Rotational speed Ω (RPM)	4000, 6000:1000:10000
Rotor axis to freestream angle α (deg)	0, 10, 20
Rotor diameter D (cm)	15.24

Table 1 Test cases for thrust measurements

2.3 Flow measurements

Particle Image Velocimetry (PIV) is employed to study the propeller flow field under pure axial descent and oblique descent. The ideal condition would be to obtain the velocity field in the mid-plane of the rotor, that is the plane containing the axis of the rotor. Nevertheless, this plane can be problematic for planar PIV measurements because of shadows by the propeller structure. For this reason, the laser sheet does not contain the axis of the propeller and it is shifted by ca. 2.5 cm to avoid too wide dark areas.

Two different tracer particles are employed. First of all, micron sized droplets of glycol-water solution are injected in the wind tunnel through a SAFEX fog generator, which provided of particles with a diameter of about 0.1 μm. The use of fog droplets to study axial descent limited the field of view to a maximum of 25x25 cm^2. For this reason, the oblique descent was approached by changing the seeding to Helium Filled Soap Bubbles (HFSB, (Caridi, et al., 2016)). The bubbles, with a mean diameter of 0.4 mm and 10^4 times brighter, allowed to bring the field of view up to 40x40 cm^2. The particles are illuminated by a high speed laser, type Nd:YLF (25 mJ), which can reach 10 kHz of repetition rate and a pulse width < 200 ns. The imaging system consists of a Photron FASTCAM SA1.1. The high speed CMOS camera is provided with a lens with a focal depth of 50 mm (for fog droplets) and 60 mm (for HFSB). The maximum resolution is 1024×1024 at 5.4 kHz. System synchronization is obtained with a LaVision Programmable Timing Unit (PTU X). The measurements in axial descent are obtained with the camera set in double frame (dt 300 μs, max particle displacements of 9 px) at a rate of 200 Hz for 2 seconds, giving 400 image pairs. For the oblique descent 2500 images

are acquired at a rate of 5 kHz, in single frame. The data from these acquisitions provide an average flow field over 0.5 sec, but allow to perform some flow visualizations to qualitatively understand the characteristic phenomena of the flow around the propeller. The raw image is pre-processed by subtracting the minimum over 7 subsequent images to reduce reflections from the propeller support. PIV is then performed using interrogation windows size of 32x32 pixels/mm for the fog particle and 48x48 pixels/mm for the HFSB. The time-averaged velocity field is computed from the mean of all instantaneous velocity fields for each test condition. The schematic for the PIV setup is shown in Figure 3 and Table 2 Table 2 summarizes the conditions studied.

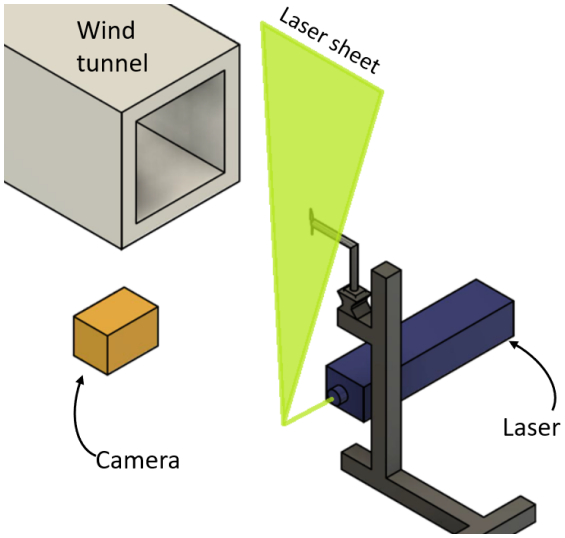

Figure 3 Schematic representation of the experimental apparatus for PIV measurements

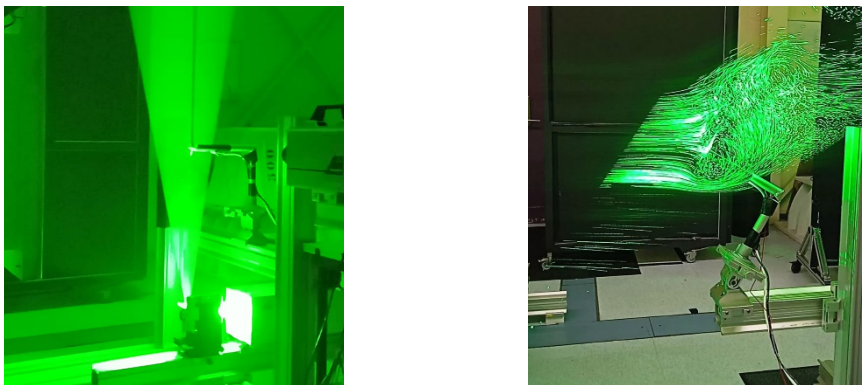

Figure 4 On the left: illuminated fog particles in the measurement domain; on the right: illuminated HFSB in the measurement domain

AXIAL DESCENT	
Parameter	**Value(s)**
Wind Tunnel Speed (m/s)	7.4, 7.7, 7.8, 8, 8.1, 8.6, 9.8, 11, 12.1, 13.3
Propeller RPM	8000
Descent angle α (deg)	0

OBLIQUE DESCENT	
Parameter	**Value(s)**
Wind Tunnel Speed (m/s)	6.8, 7.4, 8, 8.6
Propeller RPM	8000
Descent angle α (deg)	0:10:30

Table 2 Oversight of test conditions for axial descent and oblique descent

3 Experimental Results and Discussion

3.1 Thrust measurements

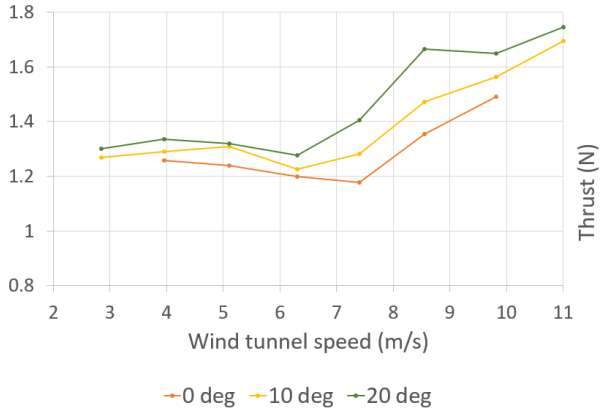

Figure 5, left, collects all the curves that were obtained during the measurements. The shape of the curves seems to be in line with the general trends that were found in literature (Betzina, 2001), (Yaggy & Mort, 1963) and with the explanation of thrust behaviour in (Brand, et al., 2011). After an initial phase of slow descent, where we see a slight increase of thrust for the higher RPM by an increase in local blade angle, it is plausible to think that the propeller gets closer to the vortex rings region as the thrust experiences a loss. This reduction in thrust is also influenced by the propeller rotational speed, the trend of which is highlighted by the red dotted line. Another interesting point is that the zone where the thrust decreases is then followed by an increase of the thrust. In this region it was also registered an increase of current of the power supply used to move the motor of the propeller. Considering that the voltage was kept fixed, this increase could be explained with an increase of power required to maintain the RPM constant in a fast descent. Moreover, in this condition the blades are most likely completely stalled, thus the force measured by the load cell may be an increase of drag due to the stall which is measured as an axial force. The black circles are the wind tunnel speed at which following flow measurements results will be shown.

Thrust measurements are also pursued for oblique descent conditions. The results of this process can be found in Figure 5, right. From the diagram, it seems that the 20° case has a less severe loss of thrust compared to the other configurations. Nevertheless, these acquisitions should be better and more thoroughly investigated as the thrust sensor seems to be less reliable in steep descent conditions. The same test executed two different times could return measurements with a difference of about 15%. The cause of this behaviour is not clear: it could be due to the acquisition system cables not correctly stored, temperature changes, possible increase of level of vibration of the support.

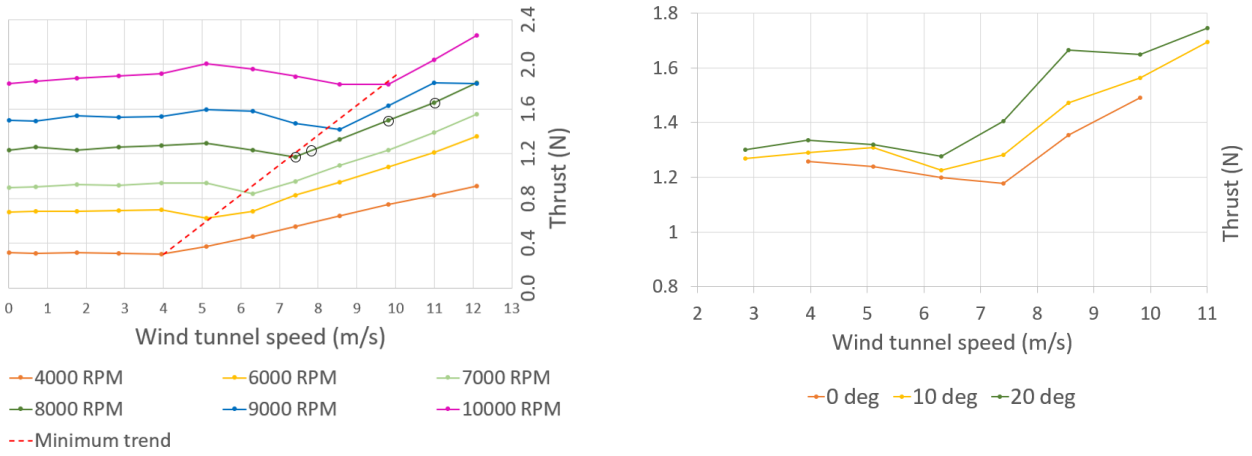

Figure 5 On the left: curves at various descent speed (wind tunnel speed) V_∞ and propeller RPM, axial descent; on the right: curves at various descent speed and descent angle, with Ω = 8000 RPM

3.2 Flow measurements

In test conditions of axial descent it is possible to observe the beginning of the re-ingestion of the wake in Figure 6a, as recirculating patterns form around the blade tips. If the wind tunnel speed is increased, it is expected that the stagnation point as well as the whole recirculating pattern move towards positive x-direction (Figure 6b and c). In fast descent an increase of current was registered and this was justified with the electrical motor which keeps the RPM fixed even at high values of the wind tunnel speed. The fact that Ω is held fixed to 8000 RPM means that the propeller does not enter the autorotation condition and the flow does not pass "through" the disc. This is supported by the velocity field obtained through PIV measurements in fast descent conditions (Figure 6d).

Streak visualizations are performed to visualize the bubble-like structure which forms around the propeller. The maximum intensities in 21 subsequent images are overlapped time to time (4 ms). This was useful to visualize the burst of the bubble around the propeller, in Figure 7. It is possible to observe how the stagnation point moves when the bubble starts to build up (Figure 7a and Figure 7b).

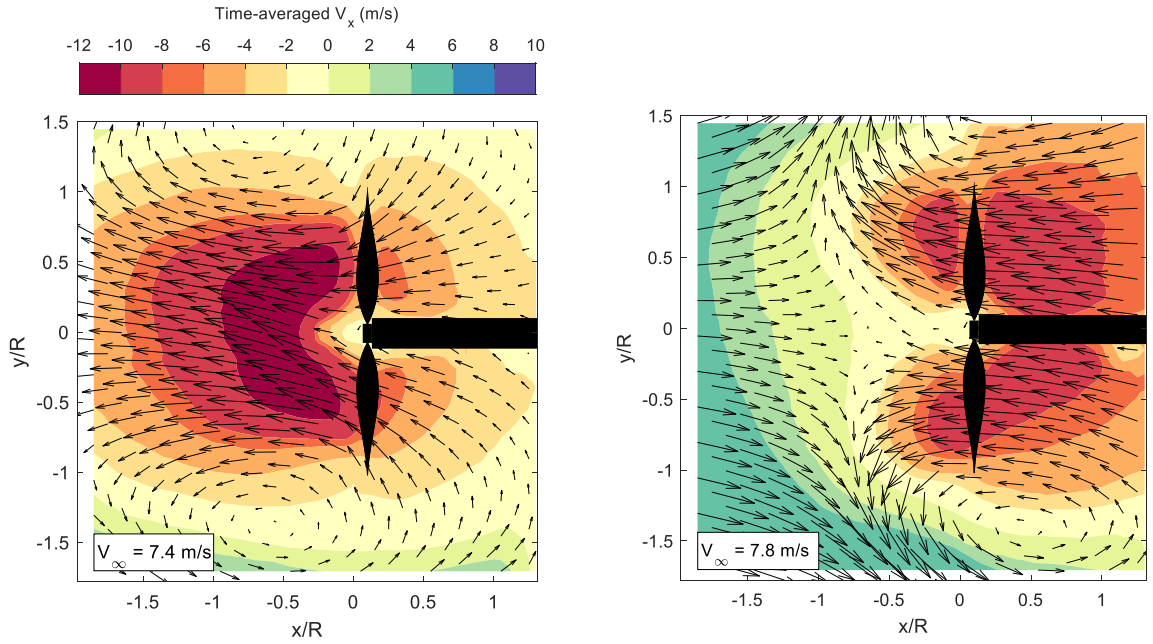

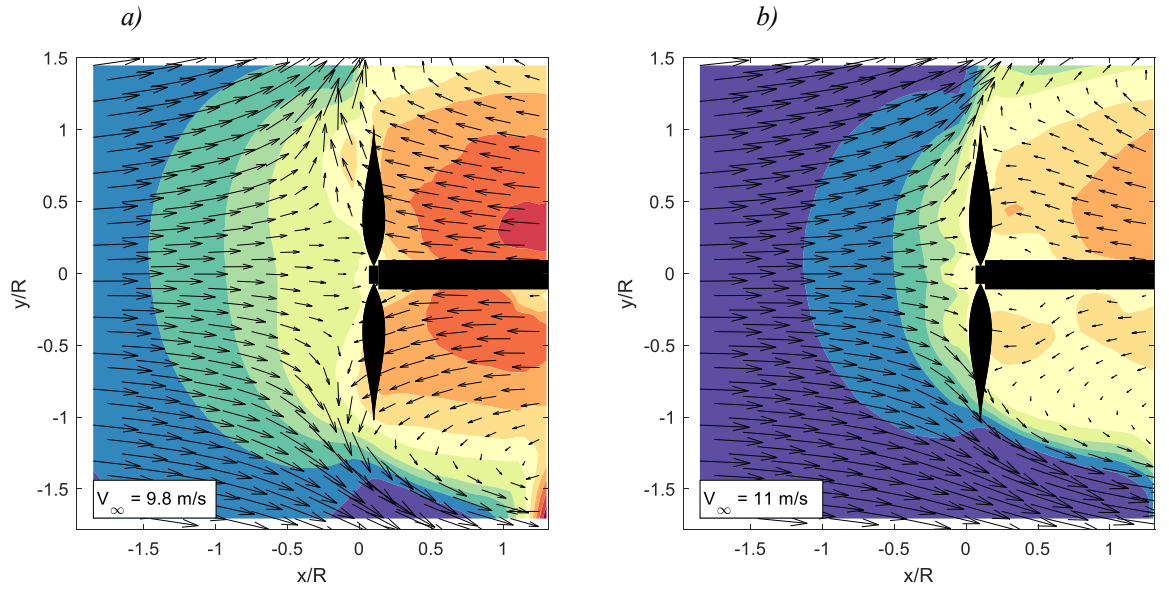

Figure 6 Propeller in descent at several descent speed. Time-averaged velocity field (x component) and 2D vectors, Ω=8000 RPM. The three conditions are those represented with black circles in Figure 5, left

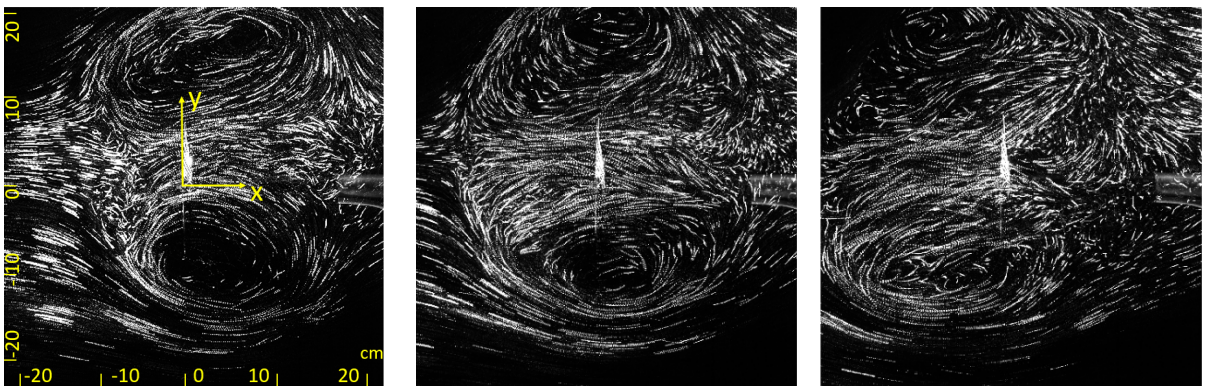

a) $t = 0$ *ms* *b)* $t = 64$ *ms* *c)* $t = 152$ *ms*

Figure 7 Time sequence of HFSB streaklines in VRS (axial descent). Build up and burst of the bubble, $V_\infty = 7.4\ m/s$

After having studied the axial descent and the formation-destruction of the bubble-like structure, the next step is giving a descent angle to the configuration and analyse what happens to the flow. At a small descent angle of 10° the flow pattern presents the re-ingestion of the wake through the rotor around both blades and a bubble-like body begins to form, as in axial descent. The destruction of the bubble though is more prone to occur on the "upper" blade (y-direction, see Figure 7a). The bubble collapses on one side while the ring installed around the lower blade moves back and forth (Figure 8a). When the descent angle is increased to 20° (Figure 8b), the asymmetrical explosion of the bubble occurs much earlier: the vortices that accumulate around the upper blade are rapidly ejected. At 30° (Figure 8c) the bubble does not even form: the ring around the upper blade is blown away as soon as it forms. This phenomenon can

be observed multiple times in the 0.5 s window, while the creation-destruction cycle of the bubble is axial descent requires few seconds.

a) $\alpha = 10°$ b) $\alpha = 20°$ c) $\alpha = 30°$

Figure 8 Time sequence of HFSB streaklines in VRS (oblique descent) for various descent angles, $V_\infty = 7.4\ m/s$

The observations proposed for the streak visualizations are supported by the PIV measurements in Figure 9, where the time-averaged velocity field is shown. The freestream velocity is the same as in Figure 6a, allowing a comparison between axial descent and oblique descent. At $\alpha = 10°$ (Figure 9a) the stagnation point moves downward, out of the propeller axis and the reduction of velocity is more severe on the lower blade. The wake is moving upwards, more evident at $\alpha = 20°$ (Figure 9b), while the stagnation point is shifting towards the disc and the recirculation zone downstream. It is possible to see how the ring on the lower blade is basically behind the disc. This is also true at $\alpha = 30°$ (Figure 9c), where a ring on the upper blade is not even present.

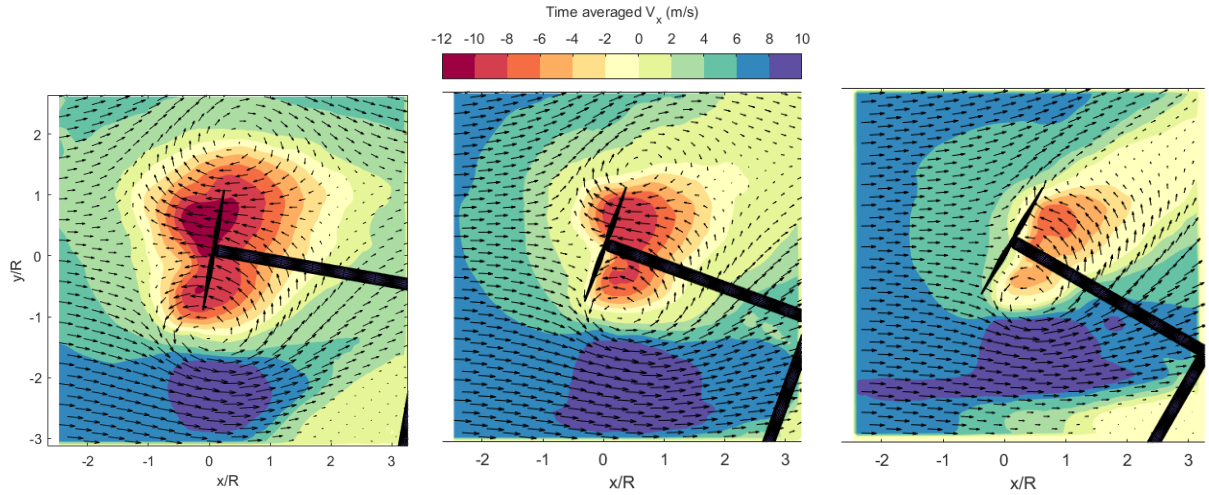

a) $\alpha = 10°$ b) $\alpha = 20°$ c) $\alpha = 30°$

Figure 9 Propeller in oblique descent. Time-averaged velocity field (x component) and 2D vectors, Ω=8000 RPM, $V_\infty = 7.4\ m/s$

4 Vortex Ring State Modelling

The results from PIV measurements are exploited to understand the behaviour of a VTOL aircraft (i.e., a helicopter) in descending flight. The induced velocity at several wind tunnel speeds V_∞ and angle of descent α is evaluated near the disc. Following Glauert's approach for the actuator disc theory in forward flight, induced velocity is calculated

considering that in the proximity of the disc the velocity field from PIV measurements is the sum of the wind tunnel speed V_∞ and the induced velocity v_i. In forward flight (i.e., having an oblique descent), the induced velocity is obtained through the projection of V_∞ normal to the rotor disc (Figure 10). The theoretical and experimental induced velocity are shown in Figure 11, where $v_{ih} = \sqrt{\frac{T}{2\rho A}}$ is the induced velocity in hover evaluated through actuator disc theory (T=W thrust equals weight in hover, A disc area). According to theory, the "region of roughness" where the rotor is in VRS corresponds to a rate of descent $-2 < \frac{V_z}{v_{ih}} < 0$. In this state, the high rate of descent has overcome the normal downward induced flow on inner blade sections and the flow is stagnating at the level of the rotor. The experimental results plotted in Figure 11 show that this is the case as the induced velocity increases more than expected as compared to the theory, as supported in (Brand, et al., 2011), due to the accumulation of vortices near the disc. The peak of v_i is lower at higher descent angles, as vortices are rapidly "blown away" due to forward speed. In the equations of motion, the induced velocity will be normalized with respect to the blade tip speed, thus $\lambda_i = \frac{v_i}{\Omega R}$.

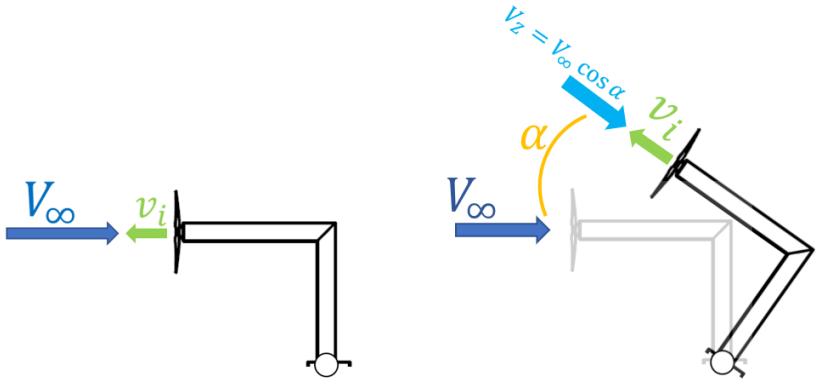

Figure 10 Wind tunnel speed and induced velocities (axial and oblique descent)

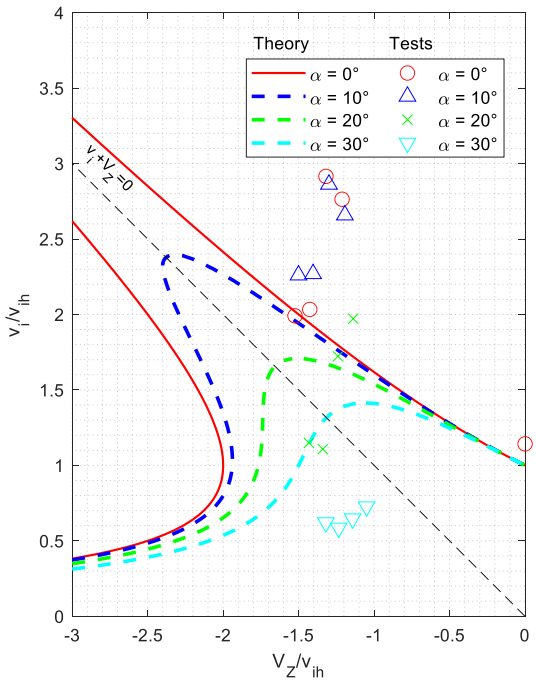

Figure 11 Non-dimensional induced velocity $\frac{v_i}{v_{ih}}$ at several descent rates $\frac{V_z}{v_{ih}}$ (V_z velocity normal to the disc). Comparison between Glauert's theory in forward flight and wind tunnel tests

The theoretical 3DOF longitudinal equations of motion are first used to simulate a descent and results are shown in Figure 12, left hand-side. In this figure the model is using a first order quasi-dynamic inflow model without accounting for the VRS experimental results of Figure 11. The u and w velocities are with respect to the body-axes, which in our case can be considered the horizontal V_X and vertical V_Z components. Rotational speed is held constant. A linear interpolation between the values from the tests is adopted.

The vehicle starts from hovering condition. After 2 s the collective is decreased from $\theta_0 = 5.2°$ to $\theta_0 = 4.5°$ and the helicopter begins to descend. While descending, the induced velocity is increasing according to the linear interpolation between the values from experimental tests in Figure 11 (as shown by the parameter $\lambda_i = \frac{v_i}{\Omega R}$ in Figure 12) and the helicopter keeps on descending, possibly entering VRS. At $t = 3s$ the collective pitch is increased to the initial value. After having increased the collective, if VRS is not considered, it is expected that the vehicle is able to recover and arrest its descent as with the model in (Pavel, 2001), Figure 12, right. What happens, though, is that the helicopter is not able to recover and keeps on descending even faster. If higher collective is provided, it is possible to see that the helicopter is able to recover, but in reality high values of collective might not be available.

The data of the vehicle used in the simulation are as following: M = 2200 kg vehicle mass, moment of inertia I_{yy} = 4892 kg m^2, fuselage drag considered as flat plate area CD ∗ S = 1.5, rotor radius R = 7.32 m, rotor rip velocity V_{tip} = 200 m/s, lift coefficient $C_{l\alpha} = 5.7$ deg^{-1}, vertical distance from rotor hub to vehicle CG h = 1m, blade solidity $\sigma = 0.075$, Lock number $\gamma = 6$.

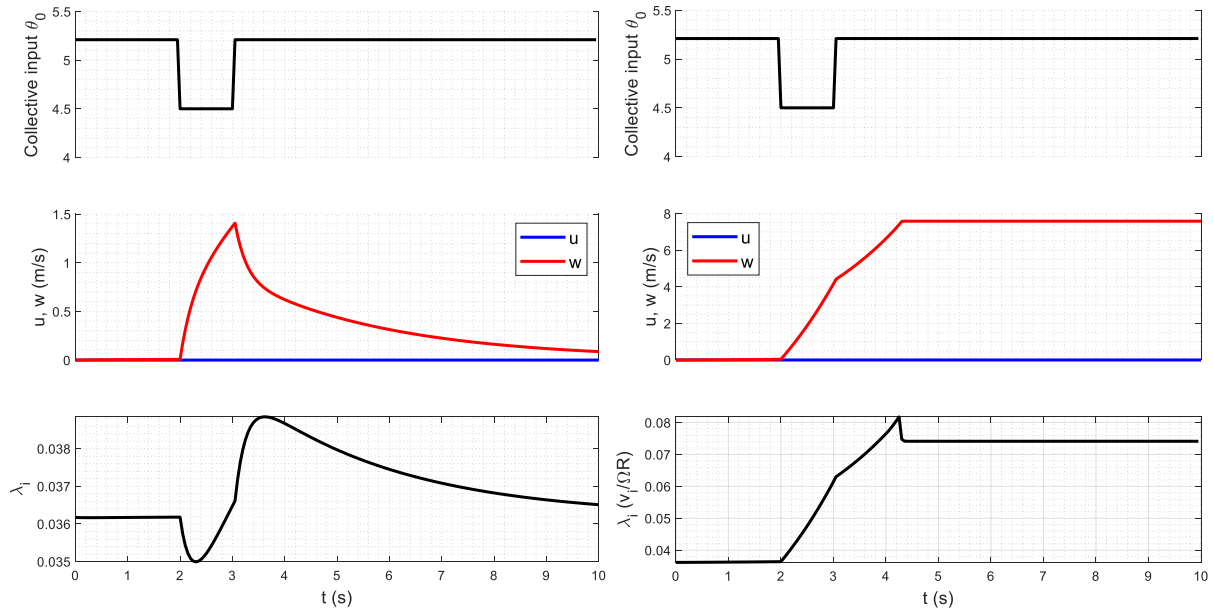

Figure 12 Helicopter response to a decrease of collective. On the left: v_i (λ_i) from quasi-steady dynamic inflow by means of a time constant τ of value 0.1, $\dot{\lambda}_i = \frac{C_{T,BEMT} - C_{T,Glauert}}{\tau}$; on the right: v_i (λ_i) from tests

5 Conclusion

An experimental study was conducted to investigate the VRS a propeller experiences in descent. Thrust and flow measurements through load cell respectively PIV technique were performed in the low speed wind tunel at Delft University of Technology. This allowed to obtain information regarding both the thrust and the flow pattern, showing the characteristic decrease of thrust, followed by an increase of power required to maintain the RPM fixed, and re-ingestion of the wake through the disc. Unsteady phenomena were observed during the tests, during both axial and

oblique descent. In axial descent the formation-destruction of the "bubble-like" structure was observed, noticeable also though the movement of the stagnation point. In oblique descent at low angles (ie., 10°) the bubble forms and is prone to burst on one side only. At higher angles, the bubble was highly unstable and the vortices that attempt to pile up near the disc were rapidly ejected. The induced velocity in axial descent exihibit an increase of 50% with respect to Glauert's actuator disc theory, at descent speeds between ca. 1-1.5v_{ih}, due to the accumulation of vortices in VRS. This translated into an increase of collective required to arrest the vehicle descent after having entered VRS.

References

Azuma, A. & Obata, A., 1968. Induced Flow Variation of the Belicopter Rotor Operating in the Vortex Ring State. *Journal of Aircraft,* 5(4), pp. 381-386.

Basset, P.-M. & Prasad, J. V. R., 2002. *Study of the Vortex Ring State Using Bifurcation Theory.* American Helicopter Society 58th Annual Forum, Montréal, Canada

Betzina, M. D., 2001. *Tiltrotor Descent Aerodynamics: A Small-Scale Experimental Investigation of Vortex Ring State.* American Helicopter Society 57th Annual Forum, Washington D.C., Vertical Flight Society.

Brand, A., Dreier, M., Kisor, R. & Wood, T., 2011. The nature of Vortex Ring State. *Journal of the American Helicopter Society,* 56(2), p. 22001.

Caridi, G. C. A., Ragni, D., Sciacchitano, A. & Scarano, F., 2016. HFSB-seeding for large-scale tomographic PIV in wind tunnels. *Experiments in Fluids,* 57(12), pp. 1-13.

Glauert, H., 1926. *The Analysis of Experimental Results in the Windmill Brake and Vortex Ring State of an Airscrew, Aeronautical Research Council, Reports and Memoranda, n° 1026,* London: Her Majesty's Stationery Office.

Jimenez, J., 2002. *Experimental and Numerical Study of the Helicopter Behaviour in Steep Descent and Modelling of the Vortex Ring State.* Ph.D. Dissertation, ONERA

Jimenez, J., Desopper, A., Taghizad, A. & Binet, L., 2001. *Induced velocity model in steep descent and vortex ring state prediction.* France

Jimenez, J., Taghizad, A. & Binet, L., 2002. *Helicopter Flight Tests in Steep Descents: Vortex-Ring State Analysis and Induced Velocity Models.* Cambridge, UK

Meijer Drees, J. & Hendal, W. P., 1950. *The field of flow through a helicopter rotor obtained from wind tunnel smoke tests.* Amsterdam: NLL.

Meijer Drees, J. & Hendal, W. P., 1951. Airflow patterns in the neighbourhood of helicopter rotors. *Aircraft Engineering and Aerospace technology,* 23(3), pp. 107-111.

Newman, S. et al., 2003. Predicting the Onset of Wake Breakdown for Rotors in Descending Flight. *Journal of the Americal Helicopter Society,* Volume 48, pp. 28-38.

Pavel, M. D., 2001. *On the Necessary Degrees of Freedom for Helicopter and Wind Turbine Low-Frequency Mode-Modeling,* Ph. D. Dissertation. Delft university of Technology

Peters, D. A. & Chen, S. Y., 1982. Momentum theory, dynamic inflow, and the. *Journal of the American Helicopter Society*, Volume 27.

Prasad, J. V. R. & Chen, C., 2005. *A Simplified Inflow Model of a Helicopter Rotor in Forward Descent.* 43rd AIAA Aerospace Sciences Meeting and Exhibit, Atlanta

Reeder, J. P. & Gustafson, F. B., 1949. *On the Flying Qualities of Helicopters,* Washington: Work of the US Gov..

Stewart, W., 1959. *Helicopter Behaviour in the Vortex-Ring State Conditions, Aeronautical Research Council Reports & Memoranda, n° 3117.* London: Her Majesty's Stationery Office.

Talaeizadeh, A., Antunes, D., Pishkenari, H. N. & Alasty, A., 2020. Optimal-time quadcopter descent trajectories avoiding the vortex ring and autorotation states. *Mechatronics,* 68(102362).

Washizu, K., Azuma, A., Koo, J. & Oka, T., 1966. Experiments on a Model Helicopter Rotor Operating in Vortex Ring State. *Journal of Aircraft,* Volume 3.

Wolkovitch, J., 1971. Analytical prediction of vortex-ring boundaries for helicopters. *Journal of the American Helicopter Society,* 17(3), pp. 13-19.

Yaggy, P. F. & Mort, K. W., 1963. *Wind Tunnel Tests of two VTOL Propellers in Descent,* Washington, D.C: s.n.